period between 3 weeks and 8 weeks post-irradiation (Fig. 5B). At 8 weeks post-irradiation, the BMDM density in the brain stem was 1.5 times and 3.3 times higher than that observed in the basal ganglia and cerebral cortex, respectively. There were statistically significant differences in BMDM density between the brain stem or basal ganglia and cerebral cortex at 8 weeks post-irradiation (Fig. 5B). Thus, following cranial irradiation, BMDM were induced most densely in the brain stem, followed by the basal ganglia and cerebral cortex during our 8-week observation period.

DISCUSSION

Although hematopoietic progenitor cells differentiate into microglia in the prenatal state [4], whether this occurs in the adult brain remains an unanswered question.

Priller *et al.* investigated whether microglia originated from hematopoietic cells during transient focal cerebral ischemia in mice that received transplantation of GFP-labeled BM cells after sublethal irradiation [5]. They showed that a massive infiltration of GFP-labeled round-shaped cells occurred in the ischemic cortex, striatum and hippocampus 24 h after transient middle cerebral artery occlusion. Donor BM-derived cells that had infiltrated the wounded parenchyma were shown to differentiate into Iba1-positive microglia. The authors also evaluated CNS microglial engraftment in a more selective lesion model, namely, transection of the fimbria-fornix. They obtained essentially the same result with this model [5]. These results reveal an enhanced microglial engraftment following CNS injury, which likely suggests mechanical destruction of the blood–brain barrier (BBB) as a promoting factor for the migration of BM cells into the brain. On the other hand, Priller *et al.* also applied unilateral facial nerve axotomy, which leaves the BBB intact, and ramified GFP-expressing cells were found to ensheath the axotomized motoneurons in the facial nucleus [5]. Collectively, they proposed that neurons might signal damage to circulating cells via specific molecular mediators, such as monocyte chemoattractant protein-1, as a mechanism by which BMDM is induced in the brain.

Although there are several studies showing the presence of BMDM in the adult brain [5, 6, 10, 11], it remains unclear whether BM transplantation, irradiation or both induce BMDM migration into the brain tissue because previous studies used BM transplantation to selectively label BM cells with GFP along with sublethal whole-body irradiation pretreatment. Sublethal whole body irradiation could cause inflammatory changes in many organs and tissues [12], leading to the release of various cytokines [13, 14]. Cytokines may subsequently affect the transplanted BM cells, potentially contributing to the induction of BMDM in the brain. Alternatively, allogeneic BM cells may trigger immune responses in the brain tissue, where they, in turn, receive signals driving their differentiation into BMDM [15, 16]. Thus, it remains unsolved whether cranial irradiation alone has the potential to induce BMDM in the brain.

In the present investigation, we addressed this question using MSCV-GFP mice that selectively express GFP in BM cells but not in the brain [8], with the exception of cerebellar Purkinje cells [8]. This expression did not interfere with the detection of BM-derived microglia. Therefore, the use of MSCV-GFP mice allowed us to examine the influence of cranial irradiation on BMDM induction without BM transplantation. Our results showed that the cranial irradiation of MSCV-GFP mice induced migration of endogenous (GFP-labeled) BM cells into numerous regions in the brain (in particular, the brain stem, basal ganglia, and cerebral cortex). The migrated BM cells were immunolabeled for Iba1, indicating that they were microglia in nature. BM cells entered the brain presumably due to the destruction of the BBB, and the BM cells differentiated into microglia, most likely via molecular mediators produced following brain injury. Although the mechanism of BMDM induction remains unclear, the present study clearly shows that cranial irradiation alone is sufficient to induce BMDM.

Burrell *et al.* studied the time-course of BMDM migration in the brain tissue from 1 d to 3 weeks after cranial irradiation in mice treated with both BM reconstitution and irradiation. The authors found that the number of BMDM increased over time until 3 weeks [6]. Our results showed that BMDM continued to increase in number up to 8 weeks post-irradiation, and at this time, the BMDM density was significantly higher than that observed at 3 weeks in the three brain regions examined. In contrast, there was no statistically significant difference in resident microglia density in the three brain regions between 3 weeks and 8 weeks after cranial irradiation (Fig. 5). These observations suggest that resident microglia migrate to target sites within 3 weeks after irradiation, whereas migration of BMDM to the brain tissue occurs continuously over a longer period. Priller's previous study [5] showed that migration of BMDM to the brain tissue continued to increase for up to 15 weeks. In this context, it is possible that resident microglia are induced into the injured sites relatively quickly, and then BMDM migrate gradually to the same sites over a longer time-span.

Regarding the relationship between apoptosis and recruitment of BMDM, apoptosis is reported to be found with high frequency 1 d after cranial irradiation in brain parenchyma, and diminished in a time-dependent manner by 21 d after irradiation [6]. We also examined apoptosis under our irradiation condition and got basically the same result. Although there were no cleaved caspase-3-positive cells in sections from non-irradiated MSCV-GFP mice, the cleaved caspase-3-positive cells were observed in sections from irradiated MSCV-GFP mice at 3 weeks after cranial irradiation, thereafter these cells almost disappeared at 8 weeks after cranial irradiation (data not shown). Thus, the recruitment of BMDM seems to continue after the disappearance of apoptotic cells.

Migration of BMDM may similarly be induced in human patients following brain irradiation. Whether BMDM have similar roles as resident microglia, and what the slower accumulation time-course of BMDM compared with resident microglia in the damaged areas means, are questions that remain unsolved. Given that BMDM play roles similar to those of resident microglia, BMDM could have significant therapeutic potential in neuronal tissues damaged by neurodegenerative diseases or brain tumors [1–3]. Moreover, cranial irradiation could induce other types of cells from bone marrow including stromal cells. Further studies are required to clarify mechanisms and the pathophysiological significance of BMDM and other types of bone marrow-derived cells in the irradiated brain.

ACKNOWLEDGEMENTS

We would like to thank to Junko Sugiyama for technical assistance. This work was presented in part at the 11th International Stereotactic Radiosurgery Society Congress, 2013, Toronto, Canada.

FUNDING

This work was supported by the Funding Program for Next Generation World-Leading Researchers (LS021) (to H.H.). In addition, it was supported by Grants-in-Aid from the Ministry of Education, Culture, Sports, Science and Technology of Japan for Scientific Research in Innovative Areas and from the Japan Society for the Promotion of Science for Young Scientists (to T.K.). Funding to pay the Open Access publication charges for this article was provided by Gunma University.

REFERENCES

1. Bauer J, Sminia T, Wouterlood FG *et al.* Phagocytic activity of macrophages and microglial cells during the course of acute and chronic relapsing experimental autoimmune encephalomyelitis. *J Neurosci Res* 1994;**38**:365–75.
2. Grenier Y, Ruijs TC, Robitaille Y *et al.* Immunohistochemical studies of adult human glial cells. *J Neuroimmunol* 1989;**21**: 103–15.
3. Wake H, Moorhouse AJ, Jinno S *et al.* Resting microglia directly monitor the functional state of synapses *in vivo* and determine the fate of ischemic terminals. *J Neurosci* 2009;**29**: 3974–80.
4. Ginhoux F, Greter M, Leboeuf M *et al.* Fate mapping analysis reveals that adult microglia derive from primitive macrophages. *Science* 2010;**330**:841–5.
5. Priller J, Flügel A, Wehner T *et al.* Targeting gene-modified hematopoietic cells to the central nervous system: use of green fluorescent protein uncovers microglial engraftment. *Nat Med* 2001;**7**:1356–61.
6. Burrell K, Hill RP, Zadeh G. High-resolution *in-vivo* analysis of normal brain response to cranial irradiation. *PLoS One* 2012;**7**:e38366. doi: 10.1371/journal.pone.0038366.
7. Ramezani A, Hawley TS, Hawley RG. Lentiviral vectors for enhanced gene expression in human hematopoietic cells. *Mol Ther* 2000;**2**:458–69.
8. Oue M, Handa H, Matsuzaki Y *et al.* The murine stem cell virus promoter drives correlated transgene expression in the leukocytes and cerebellar Purkinje cells of transgenic mice. *PLoS One* 2012;**7**:e51015. doi: 10.1371/journal.pone.0051015.
9. Nakamura K, Kosugi I, Lee DY *et al.* Prolyl isomerase Pin1 regulates neuronal differentiation via β-catenin. *Mol Cell Biol* 2012;**32**:2966–78.
10. Ajami B, Bennett JL, Krieger C *et al.* Local self-renewal can sustain CNS microglia maintenance and function throughout adult life. *Nat Neurosci* 2007;**10**:1538–43.
11. Mildner A, Schmidt H, Nitsche M *et al.* Microglia in the adult brain arise from Ly-6ChiCCR2+ monocytes only under defined host conditions. *Nat Neurosci* 2007;**10**:1544–53.
12. Li YQ, Chen P, Haimovitz-Friedman A *et al.* Endothelial apoptosis initiates acute blood-brain barrier disruption after ionizing radiation. *Cancer Res* 2003;**63**:5950–6.
13. Siegal T, Pfeffer MR, Meltzer A *et al.* Cellular and secretory mechanisms related to delayed radiation-induced microvessel dysfunction in the spinal cord of rats. *Int J Radiat Oncol Biol Phys* 1996;**36**:649–59.
14. Davalos D, Grutzendler J, Yang G *et al.* ATP mediates rapid microglial response to local brain injury *in vivo*. *Nat Neurosci* 2005;**8**:752–8.
15. Banisadr G, Gosselin RD, Mechighel P *et al.* Highly regionalized neuronal expression of monocyte chemoattractant protein-1 (MCP-1/CCL2) in rat brain: evidence for its colocalization with neurotransmitters and neuropeptides. *J Comp Neurol* 2005;**489**:275–92.
16. Selenica ML, Alvarez JA, Nash KR *et al.* Diverse activation of microglia by chemokine (C-C motif) ligand 2 overexpression in brain. *J Neuroinflammation* 2013;**10**:86. doi: 10.1186/1742-2094-10-86.

ANTICANCER RESEARCH *34*: 5099-5104 (2014)

Dosimetric Analysis Between Carbon Ion Radiotherapy and Stereotactic Body Radiotherapy in Stage I Lung Cancer

TAKESHI EBARA[1], HIROFUMI SHIMADA[2], HIDEMASA KAWAMURA[2], KATSUYUKI SHIRAI[3], JUN-ICHI SAITO[3], MOTOHIRO KAWASHIMA[2], MUTSUMI TASHIRO[2], TATSUYA OHNO[2], TATSUAKI KANAI[2] and TAKASHI NAKANO[3]

[1]*Department of Radiation Oncology, Gunma Prefectural Cancer Center, Gunma, Japan;*
[2]*Gunma University Heavy Ion Medical Center, Gunma University, Gunma, Japan;*
[3]*Department of Radiation Oncology, Gunma University, Graduate School of Medicine, Gunma, Japan*

Abstract. *Aim: To evaluate dosimetric differences between carbon ion radiotherapy (C-ion RT) and stereotactic body radiotherapy (SBRT) for stage I non-small cell lung cancer (NSCLC). Patients and Methods: Thirteen stage I NSCLC cases were planned with C-ion RT and SBRT. Prescription of the dose and fractionation (fr) for stage IA and IB in C-ion RT were 52.8 Gy (RBE)/4fr and 60.0 Gy (RBE)/4fr, respectively and those in SBRT were 52.8 Gy/4fr and 60.0 Gy/4fr, respectively. Results: The conformity index (CI) for planning target volume of C-ion RT was significantly lower than that of SBRT. The normal lung doses in C-ion RT were significantly lower those that in SBRT. In particularly, for a larger tumor, C-ion RT was lower CI and normal lung dose than SBRT. Conclusion: C-ion RT has an advantage in both target conformity and sparing of normal lung in stage I NSCLC.*

The application of radiotherapy (RT) is based on the fundamental principle of achieving precise dose localization in the target lesion while causing minimal damage to surrounding normal tissues. Particle therapy with carbon ions or protons as well as stereotactic body radiation therapy (SBRT) appears to be effective for patients with stage I non-small cell lung cancer (NSCLC) (1-5). Particle therapy has a better dose distribution compared to photons. The physical advantage of particle therapy is that it can deliver similar or higher doses to the tumor while reducing doses to the surrounding normal tissues. This characteristic could prove beneficial in lung cancer patients with compromised pulmonary function.

Correspondence to: Takeshi Ebara, Department of Radiation Oncology, Gunma, Prefectural Cancer Center, 617-1 Takabayashinishi Ota, 373-8550 Gunma, Japan. Tel: +81 276380771, Fax: +81 276380614, e-mail: evashun1999@yahoo.co.jp

Key Words: Dosimetric analysis, carbon ion radiotherapy, stereotactic body radiotherapy, stage I non-small cell lung cancer.

Carbon ions and protons share the similar physical property of having a Bragg peak. However, there are several differences between them. For example, carbon ions show less lateral scatter than protons and distal fall-off of protons is steeper than that of carbon ions. In addition, a carbon-ion beam has high linear energy transfer (LET). Low-LET radiations such as photon and proton are less effective to hypoxic tumor cells and differences in radiosensitivity related to the cell cycle of tumor. In contrast, high-LET radiations can be effective because of the reduction of the oxygen enhancement ratio and differences in radiosensitivity related to the cell cycle of tumor (6).

Several studies have demonstrated that proton therapy (PT) was more advantageous than SBRT in reducing doses to the lung and delivering similar or higher doses to planning target volume (PTV) in treating stage I NSCLC (7-10). On the other hand, there is no report addressing the dosimetric comparisons between carbon ion radiotherapy (C-ion RT) and SBRT. Therefore, the purpose of the present study was to clarify the dosimetric differences between C-ion RT and SBRT for stage I NSCLC patients.

Patients and Methods

Patients. Data from 13 stage I consecutive cases (7 cases of stage IA and 6 cases of IB) of NSCLC were analyzed. All of them had actually undergone photon radiation therapy at our hospital.

Treatment planning. Computed tomography (CT) images for actual SBRT were used for this virtual plan study. CT scans were obtained under normal quiet breathing with 1.25-2.50-mm thickness and interval in supine position. The gross tumor volume (GTV) was delineated on serial CT images. The clinical target volume (CTV) was defined as the GTV with an 8-mm margin in all directions within lung parenchyma. The PTV was defined as the CTV with a 2-mm margin in all directions. The dose prescription for stage IA and IB in C-ion RT were 52.8 Gy (RBE) and 60.0 Gy (RBE) in 4 fractions, respectively and those in SBRT were 52.8 Gy and 60.0 Gy in 4fractions, respectively. The unit about Gy (RBE) has been described previously (11,12). The prescribed point was defined

0250-7005/2014 $2.00+.40

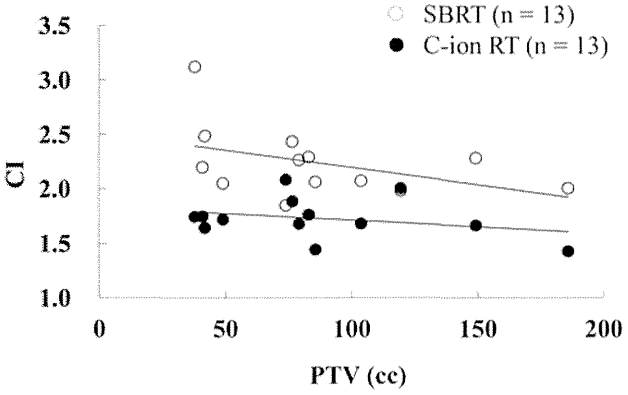

Figure 1. *Scatter diagrams comparing PTV with CI for C-ion RT and SBRT. PTV; Planning target volume, CI; conformity index, C-ion RT; carbon ion radiotherapy, SBRT; stereotactic body radiotherapy.*

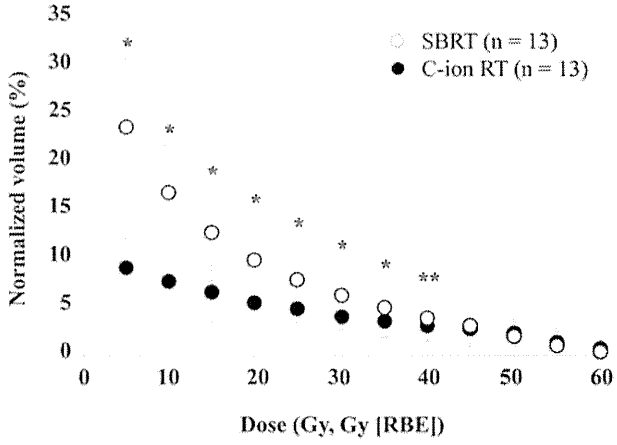

Figure 2. *The relative volumes of normal lung receiving more than a threshold dose. The differences between C-ion RT and SBRT increased with decreasing received dose. Data are presented as the mean±SD. *$p<0.001$, **$p<0.005$.*

in the center of the PTV. The same CT images and contours were used for generating the C-ion RT and SBRT. All plans were calculated with heterogeneity correction.

C-ion RT plans were designed using the XiO-N system (ELEKTA, Stockholm, Kingdom of Sweden and Mitsubishi Electric, Tokyo, Japan). The XiO-N system consists of XiO (ELEKTA)-based platform, external dose engine, k2 Dose, and connection and source data management tool (Mitsubishi Electric) and provided information necessary for a ridge filter, a range shifter, shapes of the multileaf collimator and a range compensator (RCs) bolus. The leaf margin was normally adjusted to 5-6 mm on the iso-center plane to cover the PTV with 95% of a prescribed dose. A smearing margin to the RCs to smear out the dose was added. The number of C-ion RT ports was determined to be 2 to 4 by physician's preference. The details of planning have been described previously (13).

SBRT plans were designed using the XiO 4.30 (ELEKTA) system. The shapes of beams were manually optimized using the multileaf collimation with 6 to 8 non-coplanar 4 or 6 MV photon beams. The individual field weights were also arranged in order to cover the PTV at least 80 % of the prescribed dose and minimize the organ at risk (OAR) dose.

The following dosimetric parameters were assessed; homogeneity index (HI; maximum dose/minimum dose in target) and conformity index (CI; volume receiving the minimum target dose/target volume) for the PTV. Mean normal lung dose (MLD) and Vd were evaluated by the dose-volume histogram of normal lung. Vd was defined as the relative volumes of normal lung receiving more than a threshold dose (d). For example, V20 meant the percentage of normal lung volume irradiated to 20 Gy or more. The threshold dose employed were 5–60 Gy in increments of 5 Gy. Normal lung volume was defined as the bilateral lung volume minus GTV. Maximum and mean doses to spinal cord, esophagus, trachea and heart were also evaluated.

Statistical analysis. All dosimetric data were compared with a paired two-tailed Student's *t*-test. Statistical analyses were performed using the StatView J-5.0 Japanese version software package (HULINKS, Inc. Tokyo, Japan). Differences with a *p*-value of <0.05 were considered significant.

Results

The median of GTV was 21.0 cc with a range of 4.0-66.2 cc and that of PTV was 79.1 cc with a range of 37.7-185.8 cc. The CI for PTV of C-ion RT and SBRT were 1.73±0.19 and 2.24±0.32, respectively ($p<0.01$). Figure 1 shows scatter diagrams comparing PTV with CI for C-ion RT and SBRT. Larger differences in the CI were seen with smaller PTV while C-ion RT was lower CI to larger PTV. The HI for PTV of C-ion RT and SBRT were 1.27±0.10 and 1.30±0.08, respectively (not significant). Figure 2 depicts relative volumes of normal lung receiving more than the threshold dose. V5 through V40 with increments of 5 Gy in C-ion RT were significantly lower than that in SBRT. The MLD of C-ion RT and SBRT were 2.86±1.22 Gy and 5.99±2.04 Gy, respectively ($p<0.001$). Figures 3 shows scatter diagrams comparing PTV with V5, V10, V15, V20 and MLD for C-ion RT and SBRT. The Vd and MLD of C-ion RT were lower than those of SBRT, although those for both C-ion RT and SBRT increased with enlargement of PTV. The outcomes for dosimetric parameters for normal tissues are summarized in Table I. Except for the maximum dose for the trachea, all parameters of C-ion RT were significantly smaller than that of SBRT.

Figure 4 illustrates a representative case of stage IB. C-ion RT showed that the 95% isodose line covered the PTV while SBRT showed that the 80 to 90% isodose line covered the PTV. Moreover the dose distribution outside PTV of C-ion RT is steeper than that of SBRT. In C-ion RT

Table I. *Summary of dosimetric parameters for normal tissues.*

	Maximum dose		*p*-Value	Mean dose		*p*-Value
	C-ion RT (cGy (RBE))	SBRT (cGy)		C-ion RT (cGyE (RBE))	SBRT (cGy)	
Spinal cord	2.3±2.3	12.2±7.8	0.001	0.2±0.2	2.2±1.3	0.001
Esophagus	4.1±6.9	14.4±13.3	<0.01	0.2±0.1	3.1±3.0	0.01
Trachea	19.5±24.0	21.2±22.8	NS	0.6±0.8	3.4±3.5	<0.05
Heart	7.8±19.0	15.7±19.7	<0.05	0.3±0.7	4.9±6.6	<0.05

C-ion RT: Carbon ion radiation therapy, SBRT: Stereotactic body radiotherapy. Mean±standard deviation, RBE: relative biological effectiveness.

the 50% isodose line fits to PTV and the 20% isodose line covers the half area of ipsilateral lung, while in SBRT the 50% isodose line covers the half of ipsilateral lung and the 20% isodose line covers almost all the ipsilateral lung on the iso-center plane.

Discussion

The present study revealed that C-ion RT presented a more conformal dose distribution than SBRT and significantly reduced doses to the normal tissues compared to SBRT. The characteristic carbon-ion beam, that is distal fall-off the Bragg peak and less lateral scatter than photon, realizes conformal dose distribution and sparing normal tissues. The HI for PTV showed no significant difference in C-ion RT and SBRT. Because SBRT planned to cover the almost PTV by 90 % of the prescribed dose, the dose in PTV resulted in homogeneous distribution.

There are many studies addressing the dosimetric factors to predict radiation pneumonitis (RP) in lung cancer treated with SBRT. Takeda *et al*. showed that V15 was a significant factor differentiating between grade 0-1 and grade 2 RP (14). Barriger *et al*. reported that development of symptomatic RP correlated with V20 (15). Matsuo *et al*. demonstrated that V25 was a significant factor associated with RP (16). Barriger and Borst revealed significant dose–response relationship between the risk of RP and MLD (15,17). All of these dosimetric factors were significantly low in C-ion RT compared to SBRT. Low dose parameter such as a V5, in which there was large difference between C-ion RT and SBRT has not reported the predictive value for PR after SBRT. However, the data from three-dimensional conformal radiation therapy and intensity-modulated radiation therapy for thoracic malignancies suggested that delivery of a small dose of radiation as low as 5 Gy to a large lung volume is not safe (18, 19). A small dose of radiation to a large volume of lung could be much worse than a large dose to a small volume in functional lung damage. This fact is important for candidates for radiation therapy because they have pulmonary comorbidities. Additionally, large PTV and higher CI are also reported to be significant risk factors for RP after SBRT (16, 20). C-ion RT which is keeping normal lung dose and CI at low levels could be fit for large PTV.

Although reduced doses to spinal cord, esophagus, trachea and heart were statistically significant, the absolute differences were small and with unknown clinical significance. Tolerance doses of spinal cord, esophagus and trachea were well-established and it is not difficult to establish lower tolerance doses in SBRT. On the other hand, a clear quantitative dose and/or volume dependence for most radiation-induced heart disease has not yet been shown (21). Recently, rates of major coronary events increased linearly with the mean dose to the heart by 7.4% per Gy, with no apparent threshold (22). Doses to the heart must be carefully managed because patients with stage I NSCLC are expected to be long-term survivors.

Several treatment planning studies have shown that PT demonstrates a superior conformality and a reduced dose to adjacent normal tissue or critical structures compared to SBRT (7-10). There might be no significant dosimetric difference between C-ion RT and PT for stage I NSCLC. However, the carbon-ion beam has high LET for which the relative biological effectiveness (RBE) can be as high as 2.0-3.5 (6). The tumors with low radioresponsiveness against low-LET radiations (photon and proton) are assumed to have a high proportion of hypoxic cells, poor re-oxygenation pattern and high intrinsic repair capacity. A large tumor such a T2 showed a higher local recurrence rate and worse survival than a T1 tumor. The tumor diameter was a significant factor in all failures (local, regional or distant metastases) after SBRT for stage I NSCLC (23). This can possibly be explained by the increased percentage of more radioresistant and aggressive cells in large tumors, which include larger populations of low radioresponsive cells against low LET. Thereby, it is also assumed that large tumors could benefit from C-ion RT in terms of biology.

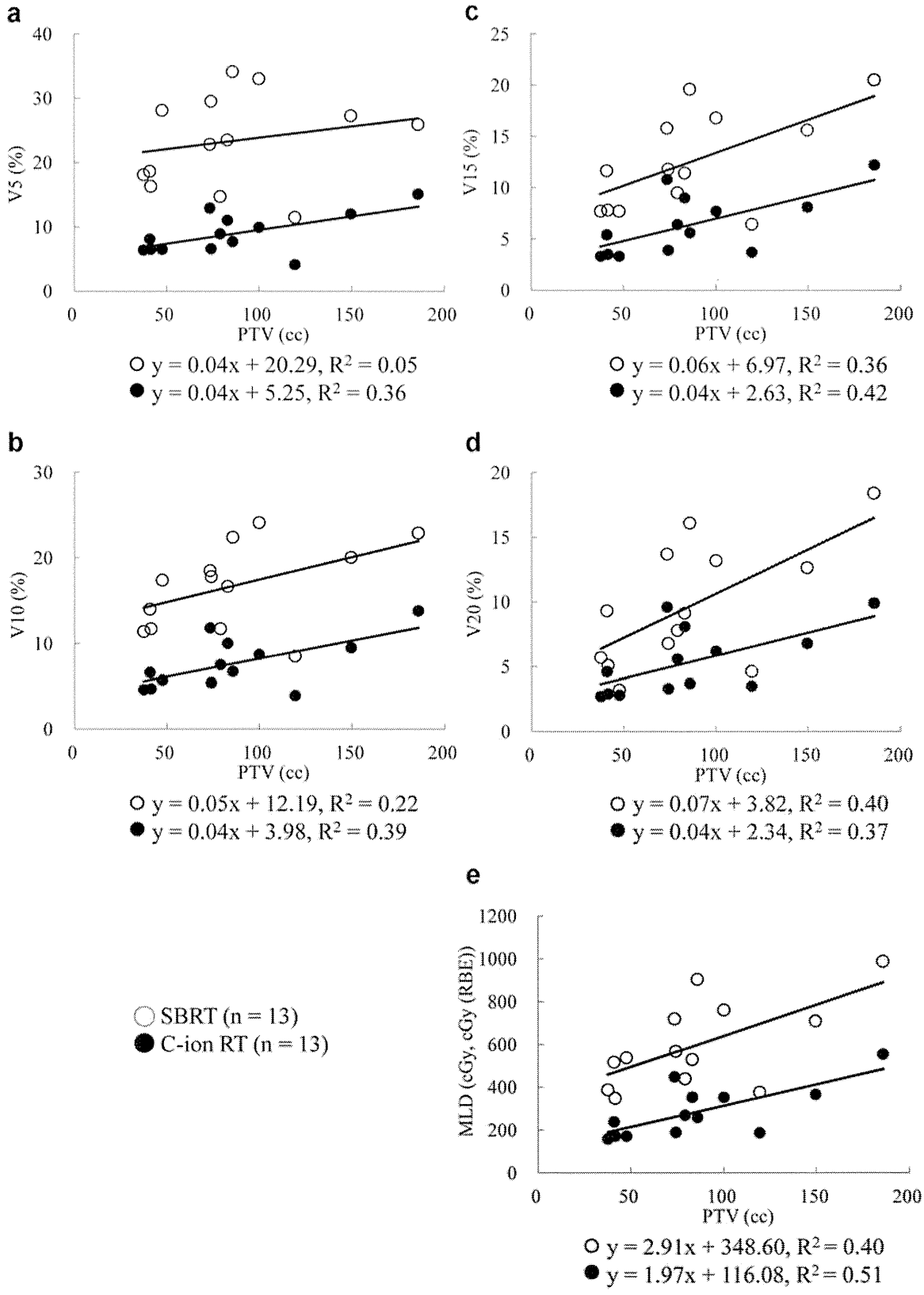

Figure 3. *(a)-(e). Scatter diagrams comparing PTV with V5, V10, V15, V20 and mean normal lung dose (MLD) for C-ion RT and SBRT.*

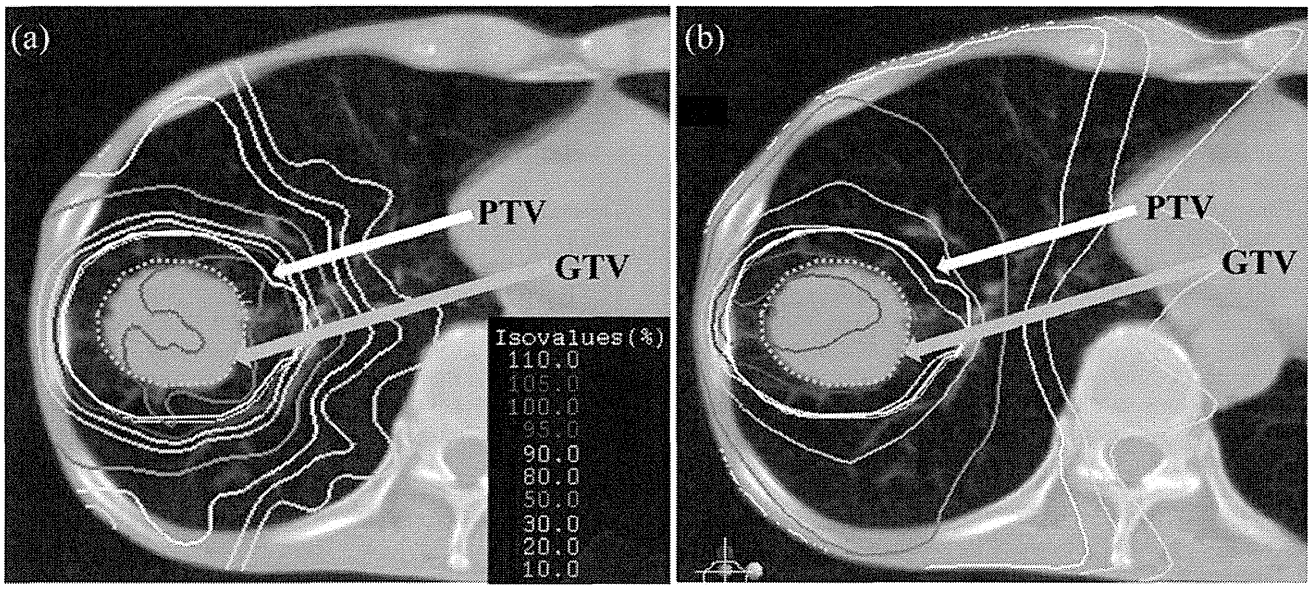

Figure 4. *(a)-(b). (a); C-ion RT, (b); SBRT). Representative case of stage IB. Color-corded dose distribution is shown with percent isodose lines.*

Finally, the limitations of the present study must be addressed. The influence of respiratory movements could not be evaluated in the present study. Because the carbon-ion beam is sensitive to geometric uncertainties and in hypodense tissue such as the lung parenchyma where the beam attenuation is low, respiratory movements are more important for the carbon-ion beam than for a photon. Strictly speaking, the tumor moves in the gating phase, although the carbon-ion beam is usually delivered under respiratory-gated movements. Because the depth dose distribution for carbon ion beam is sensitive to change in tissue density along its pathlength, intrafraction movements perturbs the carbon ion beam distribution (24). In addition, since the carbon-ion beam ports in our facility were fixed to be either horizontal or vertical, the patient was usually rolled to concentrate the dose to the target. Simulation CTs for C-ion RTs are scanned in each position because the anatomic organ location can change due to the position. However, the simulation CTs for the present study were obtained in the supine position only. Namely, the anatomic organ location changes due to the CT positions were not considered for the present study.

In conclusion, C-ion RT with 2, 3, or 4 beams provides an advantage in both target conformity and sparing of normal lung tissues compared with SBRT in peripheral stage I NSCLC. C-ion RT appears to have an advantage over SBRT especially for larger tumors.

References

1 Sugane T, Baba M, Imai R, Nakajima M, Yamamoto N, Miyamoto T, Ezawa H, Yoshikawa K, Kandatsu S, Kamada T, Mizoe J and Tsujii H: Carbon ion radiotherapy for elderly patients 80 years and older with stage I non-small cell lung cancer. Lung Cancer *64*: 45-50, 2009.

2 Miyamoto T, Baba M, Yamamoto N, Koto M, Sugawara T, Yashiro T, Kadono K, Ezawa H, Tsujii H, Mizoe JE, Yoshikawa K, Kandatsu S, Fujisawa T and Working Group for Lung C: Curative treatment of Stage I non-small-cell lung cancer with carbon ion beams using a hypofractionated regimen. Int J Radiat Oncol Biol Phys *67*: 750-758, 2007.

3 Miyamoto T, Yamamoto N, Nishimura H, Koto M, Tsujii H, Mizoe J-e, Kamada T, Kato H, Yamada S, Morita S, Yoshikawa K, Kandatsu S and Fujisawa T: Carbon ion radiotherapy for stage I non-small cell lung cancer. Radiother Oncol *66*: 127-140, 2003.

4 Miyamoto T, Baba M, Sugane T, Nakajima M, Yashiro T, Kagei K, Hirasawa N, Sugawara T, Yamamoto N, Koto M, Ezawa H, Kadono K, Tsujii H, Mizoe JE, Yoshikawa K, Kandatsu S, Fujisawa T and Working Group for Lung C: Carbon ion radiotherapy for stage I non-small cell lung cancer using a regimen of four fractions during 1 week. J Thorac Oncol *2*: 916-926, 2007.

5 Grutters JP, Kessels AG, Pijls-Johannesma M, De Ruysscher D, Joore MA and Lambin P: Comparison of the effectiveness of radiotherapy with photons, protons and carbon-ions for non-small cell lung cancer: a meta-analysis. Radiother Oncol *95*: 32-40, 2010.

6 Ohno T: Particle radiotherapy with carbon ion beams. EPMA J *4*: 9, 2013.

7 Wang C, Nakayama H, Sugahara S, Sakae T and Tokuuye K: Comparisons of dose-volume histograms for proton-beam versus 3-D conformal x-ray therapy in patients with stage I non-small cell lung cancer. Strahlenther Onkol *185*: 231-234, 2009.

8 Register SP, Zhang X, Mohan R and Chang JY: Proton stereotactic body radiation therapy for clinically challenging cases of centrally and superiorly located stage I non-small-cell lung cancer. Int J Radiat Oncol Biol Phys *80*: 1015-1022, 2011.

9 Macdonald OK, Kruse JJ, Miller JM, Garces YI, Brown PD, Miller RC and Foote RL: Proton beam radiotherapy versus three-dimensional conformal stereotactic body radiotherapy in primary peripheral, early-stage non-small-cell lung carcinoma: a comparative dosimetric analysis. Int J Radiat Oncol Biol Phys *75*: 950-958, 2009.

10 Kadoya N, Obata Y, Kato T, Kagiya M, Nakamura T, Tomoda T, Takada A, Takayama K and Fuwa N: Dose-volume comparison of proton radiotherapy and stereotactic body radiotherapy for non-small-cell lung cancer. Int J Radiat Oncol Biol Phys *79*: 1225-1231, 2011.

11 Kanai T, Endo M, Minohara S, Miyahara N, Koyama-ito H, Tomura H, Matsufuji N, Futami Y, Fukumura A, Hiraoka T, Furusawa Y, Ando K, Suzuki M, Soga F and Kawachi K: Biophysical characteristics of HIMAC clinical irradiation system for heavy-ion radiation therapy. Int J Radiat Oncol Biol Phys *44*: 201-210, 1999.

12 Kanai T, Matsufuji N, Miyamoto T, Mizoe J, Kamada T, Tsuji H, Kato H, Baba M and Tsujii H: Examination of GyE system for HIMAC carbon therapy. Int J Radiat Oncol Biol Phys *64*: 650-656, 2006.

13 Tashiro M, Ishii T, Koya J, Okada R, Kurosawa Y, Arai K, Abe S, Ohashi Y, Shimada H, Yusa K, Kanai T, Yamada S, Kawamura H, Ebara T and Ohno T and Nakano T: Technical approach to individualized respiratory-gated carbon-ion therapy for mobile organs. Radiol Phys Technol *6*: 356-366, 2013.

14 Takeda A, Ohashi T, Kunieda E, Sanuki N, Enomoto T, Takeda T, Oku Y and Shigematsu N: Comparison of clinical, tumour-related and dosimetric factors in grade 0-1, grade 2 and grade 3 radiation pneumonitis after stereotactic body radiotherapy for lung tumours. Br J Radiol *85*: 636-642, 2012.

15 Barriger RB, Forquer JA, Brabham JG, Andolino DL, Shapiro RH, Henderson MA, Johnstone PA and Fakiris AJ: A dose-volume analysis of radiation pneumonitis in non-small cell lung cancer patients treated with stereotactic body radiation therapy. Int J Radiat Oncol Biol Phys *82*: 457-462, 2012.

16 Matsuo Y, Shibuya K, Nakamura M, Narabayashi M, Sakanaka K, Ueki N, Miyagi K, Norihisa Y, Mizowaki T, Nagata Y and Hiraoka M: Dose-volume metrics associated with radiation pneumonitis after stereotactic body radiation therapy for lung cancer. Int J Radiat Oncol Biol Phys *83*: e545-549, 2012.

17 Borst GR, Ishikawa M, Nijkamp J, Hauptmann M, Shirato H, Onimaru R, van den Heuvel MM, Belderbos J, Lebesque JV and Sonke JJ: Radiation pneumonitis in patients treated for malignant pulmonary lesions with hypofractionated radiation therapy. Radiother Oncol *91*: 307-313, 2009.

18 Wang S, Liao Z, Wei X, Liu HH, Tucker SL, Hu CS, Mohan R, Cox JD and Komaki R: Analysis of clinical and dosimetric factors associated with treatment-related pneumonitis (TRP) in patients with non-small-cell lung cancer (NSCLC) treated with concurrent chemotherapy and three-dimensional conformal radiotherapy (3D-CRT). Int J Radiat Oncol Biol Phys *66*: 1399-1407, 2006.

19 Miles EF, Larrier NA, Kelsey CR, Hubbs JL, Ma J, Yoo S and Marks LB: Intensity-modulated radiotherapy for resected mesothelioma: the Duke experience. Int J Radiat Oncol Biol Phys *71*: 1143-1150, 2008.

20 Yamashita H, Nakagawa K, Nakamura N, Koyanagi H, Tago M, Igaki H, Shiraishi K, Sasano N and Ohtomo K: Exceptionally high incidence of symptomatic grade 2-5 radiation pneumonitis after stereotactic radiation therapy for lung tumors. Radiat Oncol *2*: 21, 2007.

21 Carr ZA, Land CE, Kleinerman RA, Weinstock RW, Stovall M, Griem ML and Mabuchi K: Coronary heart disease after radiotherapy for peptic ulcer disease. Int J Radiat Oncol Biol Phys 61: 842-850, 2005.

22 Darby SC, Ewertz M, McGale P, Bennet AM, Blom-Goldman U, Bronnum D, Correa C, Cutter D, Gagliardi G, Gigante B, Jensen MB, Nisbet A, Peto R, Rahimi K, Taylor C and Hall P: Risk of ischemic heart disease in women after radiotherapy for breast cancer. N Engl J Med *368*: 987-998, 2013.

23 Baumann P, Nyman J, Hoyer M, Wennberg B, Gagliardi G, Lax I, Drugge N, Ekberg L, Friesland S, Johansson KA, Lund JA, Morhed E, Nilsson K, Levin N, Paludan M, Sederholm C, Traberg A, Wittgren L and Lewensohn R: Outcome in a prospective phase II trial of medically inoperable stage I non-small-cell lung cancer patients treated with stereotactic body radiotherapy. J Clin Oncol *27*: 3290-3296, 2009.

24 Mori S, Asakura H, Kandatsu S, Kumagai M, Baba M and Endo M: Magnitude of residual internal anatomy motion on heavy charged particle dose distribution in respiratory gated lung therapy. Int J Radiat Oncol Biol Phys *71*: 587-594, 2008.

Received May 20, 2014
Revised July 7, 2014
Accepted July 9, 2014

Comparison of the radiosensitivities of neurons and glial cells derived from the same rat brain

SHIGEHIRO KUDO[1], YOSHIYUKI SUZUKI[1], SHIN-EI NODA[1], TOSHIYUKI MIZUI[2], KATSUYUKI SHIRAI[1], MASAHIKO OKAMOTO[1], TAKUYA KAMINUMA[1], YUKARI YOSHIDA[3], TOMOAKI SHIRAO[2] and TAKASHI NAKANO[1]

Departments of [1]Radiation Oncology and [2]Neurobiology and Behavior, Gunma University Graduate School of Medicine; [3]Gunma University Heavy Ion Medical Center, Maebashi, Gunma 371-8511, Japan

Received February 5, 2014; Accepted June 13, 2014

DOI: 10.3892/etm.2014.1802

Abstract. Non-proliferating cells, such as mature neurons, are generally believed to be more resistant to X-rays than proliferating cells, such as glial and vascular endothelial cells. Therefore, the late adverse effects of radiotherapy on the brain have been attributed to the radiation-induced damage of glial and vascular endothelial cells. However, little is known about the radiosensitivities of neurons and glial cells due to difficulties in culturing these cells, particularly neurons, independently. In the present study, primary dissociated neurons and glial cultures were prepared separately from the hippocampi and cerebrum, respectively, which had been obtained from the same fetal rat on embryonic day 18. X-irradiations of 50 Gy were performed on the cultured neurons and glial cells at 7 and 21 days *in vitro* (DIV). The cells were fixed at 24 h after irradiation. Terminal deoxynucleotidyl transferase-mediated dUTP nick end labeling was then performed to measure the apoptotic indices (AIs). The AIs of non-irradiated and irradiated neurons at 7 DIV were 23.7±6.7 and 64.9±4.8%, and those at 21 DIV were 52.1±17.4 and 44.6±12.5%, respectively. The AIs of non-irradiated and irradiated glial cells at 7 DIV were 5.8±1.5 and 78.4±3.3% and those at 21 DIV were 9.6±2.6 and 86.3±4.9%, respectively. Glial cells and neurons were radiosensitive at 7 DIV. However, while glial cells were radiosensitive at 21 DIV, neurons were not.

Introduction

Radiation therapy is among the essential treatment modalities for primary and metastatic brain tumors. However, subsequent cognitive function decline and developmental disorders following radiation therapy to the brain must be overcome, particularly in pediatric patients (1-5).

The central nervous system (CNS) is composed mainly of neurons, glial cells and vascular endothelial cells (Fig. 1). Neurons, the majority of which cease cell proliferation during fetal development, have been considered to be more radioresistant than glial and vascular endothelial cells, which continue to proliferate subsequent to birth. Molecular studies have provided evidence that glial cells are essential for the survival of neurons by supplying trophic factors to the neurons (6-9). Thus, the mechanism underlying the late adverse brain effects of radiation therapy has been believed to mainly be the insufficient supply of nutrients and blood to neurons due to the impaired functions of irradiated glial and vascular endothelial cells, rather than a direct effect of the radiation itself on neurons.

It was shown in the late 1990s that adult neurogenesis occurs in certain areas of the brain, including the subventricular zone (SVZ) and subgranular layer (SGL) (10). In addition, radiation-induced apoptosis of neural progenitor cells was observed in the SVZ and SGL, and relatively high radiosensitivity was demonstrated in neurons residing in the areas where neurogenesis occurs (11,12). These findings have raised the possibility that radiation-induced neuronal death may be one of the causes of the late adverse effects of radiation therapy, such as functional and developmental disorders. Therefore, attempts have been made to prevent adverse effects from developing following cranial irradiation using intensity-modulated radiation therapy to reduce the dose to areas that may be highly radiosensitive, such as the SVZ and SGL (13-16).

Radiation affects neurons and glial and vascular endothelial cells. It is therefore difficult to evaluate the radiation sensitivities of these cell types separately in *in vivo* studies. Furthermore, the majority of the previously reported *in vitro* studies were conducted on a mixture of neurons and glial cells (17). However, due to technical difficulties, only a few investigations, including our previous studies (18,19), have examined the radiosensitivity of neurons by employing monocultures of this cell type alone.

To estimate the extent of the involvement of neurons and glial cells in the adverse brain effects of radiation therapy, it

Correspondence to: Dr Yoshiyuki Suzuki, Department of Radiation Oncology, Gunma University Graduate School of Medicine, 3-39-22, Showa-machi, Maebashi, Gunma 371-8511, Japan
E-mail: syoshi@gunma-u.ac.jp

Key words: neuron, glia, radiation, apoptosis

is essential to compare radiosensitivities between glial cells and neurons. A previous study using glial cells and neurons cultured separately for such a comparison demonstrated the radiosensitivity of glial cells to be comparable to that of neurons (17). However, the cells used in that study were isolated from different individuals (different genetic backgrounds) and cultured for different lengths of time (different developmental stages), such that the results are not entirely convincing. In the present study, neurons and glial cells were therefore obtained from the same rat to ensure uniform conditions (identical genetic backgrounds and developmental stages) and their radiosensitivities were investigated separately.

Materials and methods

Cell culture. The modified Banker's method was used for primary neuronal cultures (20). Briefly, cells were obtained from the hippocampi of Wistar rat fetuses (Imai Jikkendobutu Shiikujo, Saitama, Japan) at embryonic day 18, treated with trypsin and mechanically dispersed by trituration with Pasteur pipettes. The cells were then seeded at a density of 5,000 cells/cm^2 on glass coverslips coated with poly-L-lysine and cultured in minimum essential medium (MEM; Invitrogen Life Technologies, San Diego, CA, USA) for 3 h. The coverslips were then transferred to culture dishes containing a monolayer of supporting glial cells maintained in serum-free MEM supplemented with B27 (Invitrogen Life Technologies). Cytosine β-D-arabinofuranoside (Sigma, St. Louis, MO, USA) (10 μM) was added to the culture medium at 3 days *in vitro* (DIV) to inhibit glial cell proliferation. Neurons were irradiated at 7 or 21 DIV. For X-irradiation of the cells, the cover slips were transferred to another culture dish containing only medium and no glial cells. Immediately subsequent to the irradiation of the neurons, the cover slips were returned to the original culture dishes. Although the neurons were in direct contact with the glial cells, they were easily separable; thus, it was possible to irradiate and observe only neurons.

Glial cells were obtained from the cerebral cortex of the same Wistar rat fetus as that used for obtaining neurons at embryonic day 18. Briefly, the cells were treated with trypsin, dispersed by trituration with Pasteur pipettes and then seeded at a density of 5,000 cell/cm^2 on glass coverslips coated with poly-L-lysine and cultured in MEM. Four days later, the cells were again treated with trypsin, dispersed with Pasteur pipettes and then cultured in new MEM. Glial cells were also irradiated at 7 DIV or 21 DIV. For X-irradiation of the cells, the cover slips were transferred to another culture dish containing only medium and no glial cells. Following irradiation of the glial cells, the cover slips were returned to the original culture dishes.

All animal experiments were performed in accordance with the guidelines set by the Animal Care and Experimentation Committee (Gunma University, Maebashi, Japan).

Irradiation and cell fixation. At 7 and 21 DIV, neural and glial cells were irradiated with 200 kV X-rays (Siemens-Asahi Medical Technologies Ltd., Tokyo, Japan) at a dose of 50 Gy. At 24 h after irradiation, the cells were fixed in 4% paraformaldehyde for 24 h at 4°C. Non-irradiated culture cells were handled in parallel with the irradiated samples as a control.

Assessment of apoptosis. Apoptosis was determined by terminal deoxynucleotidyl transferase-mediated dUTP nick end labeling (TUNEL) assay using the ApopTag® Plus *In Situ* Apoptosis Fluorescein Detection kit (Chemicon International, Temecula, CA, USA). Fixed cells on coverslips were permeabilized in ethanol:acetic acid (2:1) for 15 min at -20°C. The cells were then washed twice with phosphate-buffered saline (pH 7.4) for 5 min and incubated with ApopTag equilibration buffer for 5 min, followed by terminal deoxynucleotidyl transferase linkage of digoxigenin-tagged dUTP to the 3'-OH termini of DNA fragments at 37°C for 60 min. The reaction was terminated at 37°C in stop/wash buffer for 30 min and the cells were then washed. Subsequent to washing, the cells were incubated with anti-digoxigenin fluorescein antibody for 30 min and the coverslips were then mounted on slides with Vectashield® Mounting Medium with DAPI (Vector Laboratories, Burlingame, CA, USA).

Evaluation method. Fluorescein-labeled cells were observed under a Zeiss Axioplan microscope (Carl Zeiss AG, Jena, Germany) equipped with a Photometrics CoolSnap FX cooled CCD camera (Photometrics, Tucson, AZ, USA) using MetaMorph software (Universal Imaging Corp., West Chester, PA, USA). Apoptotic cells were counted on each slide. The apoptotic index (AI) was calculated as the number of DAPI- and TUNEL-positive cells divided by the number of DAPI-positive cells. The cells positive for TUNEL and negative for DAPI were excluded from the calculations.

Statistical analysis. Statistical analysis was performed using StatMate software (GraphPad Software, Inc., San Diego, CA, USA). $P<0.01$, as determined using a Student's t-test, was considered to indicate a statistically significant difference. All results are shown as the mean ± standard deviation.

Results

The average numbers of neurons and glial cells counted in each coverslip were 332 (range, 211-556) and 273 (range, 131-292), respectively. Representative images of irradiated neurons are shown in Fig. 2. The AI of 7 DIV neurons was 23.7±6.7% (n=3) in the control group and significantly higher, 64.9±4.8% (n=3), in the 50 Gy irradiated group ($P<0.001$) (Fig. 3A). At 21 DIV, the AI of neurons was 52.1±17.4% (n=9) in the control group and 44.6±12.5% (n=8) in the irradiated group; no significant difference was identified in the number of apoptotic cells between the two groups ($P=0.61$) (Fig. 3B). The average AI of 7 DIV glial cells was 5.8±1.5% (n=3) in the control group and 78.4±3.3% (n=3) in the 50 Gy irradiated group (Fig. 3C), and the average AI of 21 DIV glial cells was 9.6±2.6% (n=4) in the control group and 86.3±4.9% (n=4) in the 50 Gy irradiated group (Fig. 3D). The differences between the control and 50 Gy irradiated groups were significant at 7 DIV ($P<0.001$) as well as at 21 DIV ($P<0.001$).

Comparisons at the corresponding time-points revealed both glial cells and neurons to be radiosensitive at 7 DIV,

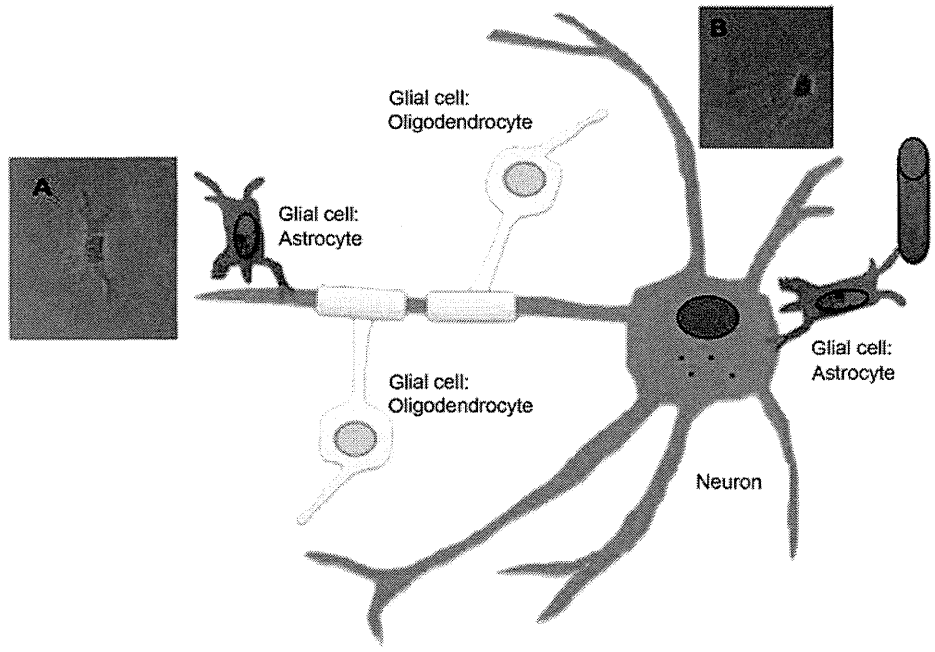

Figure 1. Illustration depicting the associations between neurons and glial cells in the CNS. The CNS is composed mainly of neurons and glial cells (astrocytes, oligodendrocytes and microglia). Glial cells are essential for the survival of neurons as they supply trophic factors to the neurons. (A and B) Phase contrast images show a (A) glial cell and (B) neuron. CNS, central nervous system. Magnification, x20.

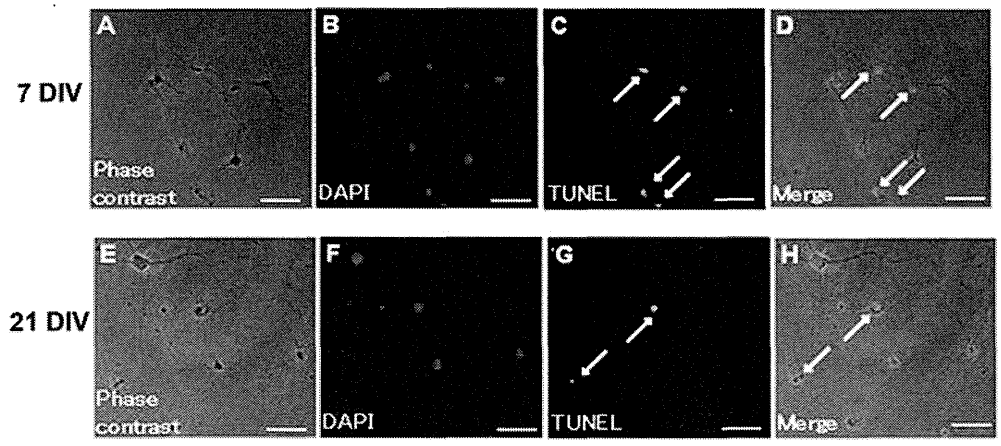

Figure 2. TUNEL analysis of cells undergoing radiation-induced apoptosis. (A-D) 7 DIV neurons; (E-H) 21 DIV neurons. (A and E) Phase contrast images; (B and F) DAPI fluorescence images; (C and G) TUNEL fluorescence images; (D and H) double fluorescence images for TUNEL (red) and DAPI (blue). Scale bar = 50 μm. DIV, days *in vitro*; TUNEL, terminal deoxynucleotidyl transferase-mediated dUTP nick end labeling. Magnification, x20. The arrows indicate nuclear pylnosis.

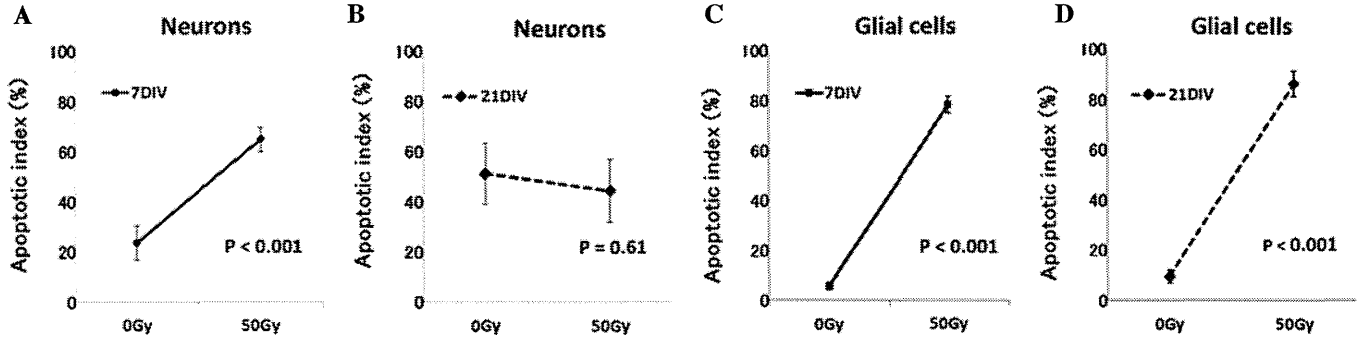

Figure 3. Plots of the average AIs of cells irradiated with 0 Gy (Control) or 50 Gy, at 7 or 21 DIV. Neurons: (A) The AI was significantly increased by 50 Gy irradiation at 7 DIV as compared with the control (n=3, P<0.001). (B) No increase in AI was identified at 21 DIV (n=8, P=0.61). Glial cells: The AI increased significantly with 50 Gy irradiation at both (C) 7 DIV and (D) 21 DIV (7 DIV, n=3, P<0.001; 21 DIV, n=4, P<0.001). The bars represent standard deviations. DIV, days *in vitro*; AI, apoptotic index.

whereas glial cells but not neurons were radiosensitive at 21 DIV.

Discussion

Our previous study revealed 7 DIV neurons (morphologically and functionally immature cells) to be relatively radiosensitive, while 21 DIV neurons (morphologically and functionally mature cells) were found to be extremely radioresistant, showing no increase in apoptosis even following high-dose irradiation (19). Furthermore, when 7 DIV neurons were exposed to low doses of X-irradiation (0, 5, 4 and 10 Gy) and further cultured for 14 and 21 days in total, the number of apoptotic cells increased, and the clustering of synaptic proteins, indicative of the maturation of synapses, decreased dose-dependently following irradiation (18). Consistent with our previous findings, the present results showed that the number of 7 DIV neurons undergoing apoptosis increased following irradiation, whereas radiation did not significantly increase apoptosis in 21 DIV neurons. These results indicate that radiosensitive immature neurons become radioresistant with maturation and that mature neurons are radioresistant.

The AI of glial cells did not differ significantly between 7 and 21 DIV in this study. Although no study has focused on the association between the maturity and radiosensitivity of glial cells, if the maturities of these cells reflect their radiosensitivity, our present results may suggest their maturities to be similar at 7 and 21 DIV. In other words, since glial cells have the ability to proliferate (gliogenesis), unlike neurons, it is assumed that a glial cell population would represent a mixture of cells with differing maturities due to this proliferation. Thus, their similar radiosensitivities suggest that the glial cells in this study may have been at similar maturation stages.

Following irradiation, glial cells may undergo mitotic cell death. Furthermore, we observed in a previous study that a large percentage of neurons underwent delayed apoptosis subsequent to irradiation (18). Thus, comparing the radiosensitivities of neurons and glial cells based on their AIs at 24 h after irradiation can be difficult. A number of studies have shown that the ability to repair radiation damage differs among sites (10,21). Eriksson *et al* (10) reported that adult neurogenesis occurs in both the SVZ and the SGL, and Seaberg *et al* (21) showed that stem cells with pluripotency and self-renewal ability were present in the SVZ, while the SGL contained predominantly neural progenitor cells without pluripotency and fewer stem cells. In other words, due to the presence of radioresistant and pluripotent stem cells in the SVZ, neurogenesis may occur following irradiation in this area, whereas recovery subsequent to irradiation may be poor in the SGL where the number of the stem cells is limited. In a study by Hellström *et al* (22), the volume and rate of DNA synthesis following whole brain irradiation were reported to be significantly higher in the SVZ than in the SGL (22). Glial cells have the ability to proliferate, such that damaged glial cells can be replaced by gliogenesis. Therefore, to understand the mechanisms underlying the adverse effects of radiation therapy on the brain, the neurogenesis, restoration of glial cells and secondary effects due to brain blood vessels being impaired by irradiation must all be taken into consideration. Furthermore, radiation effects on the brain may vary according to the irradiation site, extent and dose, due to the heterogeneous distribution of neural stem cells.

In conclusion, the radiosensitivities of neurons and glial cells, obtained from the same rat brain, were evaluated by examining the number of cells undergoing radiation-induced apoptosis. The results showed both glial cells and neurons to be radiosensitive at 7 DIV, whereas only glial cells were radiosensitive at 21 DIV; neurons exhibited radioresistance at 21 DIV. Further studies are required to elucidate the mechanisms underlying the late adverse effects of radiation therapy on the CNS.

References

1. Hall EJ and Giaccia AJ (eds): Radiobiology for the Radiologist. Sixth edition. Lippincott Williams & Wilkins, Philadelphia, PA, 2006.
2. Chang EL, Wefel JS, Hess KR, *et al*: Neurocognition in patients with brain metastases treated with radiosurgery or radiosurgery plus whole-brain irradiation: a randomised controlled trial. Lancet Oncol 10: 1037-1044, 2009.
3. Nakaya K, Hasegawa T, Flickinger JC, Kondziolka DS, Fellows-Mayle W and Gobbel GT: Sensitivity to radiation-induced apoptosis and neuron loss declines rapidly in the postnatal mouse neocortex. Int J Radiat Biol 81: 545-554, 2005.
4. Shi L, Molina DP, Robbins ME, Wheeler KT and Brunso-Bechtold JK: Hippocampal neuron number is unchanged 1 year after fractionated whole-brain irradiation at middle age. Int J Radiat Oncol Biol Phys 71: 526-532, 2008.
5. Takadera T, Sakamoto Y and Ohyashiki T: NMDA receptor 2B-selective antagonist ifenprodil-induced apoptosis was prevented by glycogen synthase kinase-3 inhibitors in cultured rat cortical neurons. Brain Res 1020: 196-203, 2004.
6. Allen NJ and Barres BA: Signaling between glia and neurons: focus on synaptic plasticity. Curr Opin Neurobiol 15: 542-548, 2005.
7. Volterra A and Meldolesi J: Astrocytes, from brain glue to communication elements: the revolution continues. Nat Rev Neurosci 6: 626-640, 2005.
8. Yamazaki Y, Hozumi Y, Kaneko K, *et al*: Direct evidence for mutual interactions between perineuronal astrocytes and interneurons in the CA1 region of the rat hippocampus. Neuroscience 134: 791-802, 2005.
9. Ye ZC and Sontheimer H: Astrocytes protect neurons from neurotoxic injury by serum glutamate. Glia 22: 237-248, 1998.
10. Eriksson PS, Perfilieva E, Björk-Eriksson T, *et al*: Neurogenesis in the adult human hippocampus. Nat Med 4: 1313-1317, 1998.
11. Peissner W, Kocher M, Treuer H and Gillardon F: Ionizing radiation-induced apoptosis of proliferating stem cells in the dentate gyrus of the adult rat hippocampus. Brain Res Mol Brain Res 71: 61-68, 1999.
12. Tada E, Parent JM, Lowenstein DH and Fike JR: X-irradiation causes a prolonged reduction in cell proliferation in the dentate gyrus of adult rats. Neuroscience 99: 33-41, 2000.
13. Barani IJ, Cuttino LW, Benedict SH, *et al*: Neural stem cell-preserving external-beam radiotherapy of central nervous system malignancies. Int J Radiat Oncol Biol Phys 68: 978-985, 2007.
14. Ghia A, Tomé WA, Thomas S, *et al*: Distribution of brain metastases in relation to the hippocampus: implications for neurocognitive functional preservation. Int J Radiat Oncol Biol Phys 68: 971-977, 2007.
15. Gutiérrez AN, Westerly DC, Tomé WA, *et al*: Whole brain radiotherapy with hippocampal avoidance and simultaneously integrated brain metastases boost: a planning study. Int J Radiat Oncol Biol Phys 69: 589-597, 2007.
16. Jaganathan A, Tiwari M, Phansekar R, Panta R and Huilgol N: Intensity-modulated radiation to spare neural stem cells in brain tumors: a computational platform for evaluation of physical and biological dose metrics. J Cancer Res Ther 7: 58-63, 2011.
17. Gobbel GT, Bellinzona M, Vogt AR, Gupta N, Fike JR and Chan PH: Response of postmitotic neurons to X-irradiation: implications for the role of DNA damage in neuronal apoptosis. J Neurosci 18: 147-155, 1998.

18. Okamoto M, Suzuki Y, Shirai K, *et al*: Effect of radiation on the development of immature hippocampal neurons in vitro. Radiat Res 172: 718-724, 2009.
19. Shirai K, Mizui T, Suzuki Y, Kobayashi Y, Nakano T and Shirao T: Differential effects of x-irradiation on immature and mature hippocampal neurons in vitro. Neurosci Lett 399: 57-60, 2006.
20. Goslin K, Asmussen H and Banker G: Rat hippocampal neurons in low-density culture. In: Banker G and Goslin K (eds): Culturing Nerve Cells. Second edition. The MIT Press, Cambridge, MA, pp339-370, 1998.
21. Seaberg RM and van der Kooy D: Adult rodent neurogenic regions: the ventricular subependyma contains neural stem cells, but the dentate gyrus contains restricted progenitors. J Neurosci 22: 1784-1793, 2002.
22. Hellström NA, Björk-Eriksson T, Blomgren K and Kuhn HG: Differential recovery of neural stem cells in the subventricular zone and dentate gyrus after ionizing radiation. Stem Cells 27: 634-641, 2009.

OPEN ACCESS Freely available online

PLOS | ONE

HLA Class I Expression and Its Alteration by Preoperative Hyperthermo-Chemoradiotherapy in Patients with Rectal Cancer

Hiro Sato[1], Yoshiyuki Suzuki[1]*, Munenori Ide[2], Toshihide Katoh[3], Shin-ei Noda[1], Ken Ando[1], Takahiro Oike[1], Yuya Yoshimoto[1], Noriyuki Okonogi[1], Kousaku Mimura[4], Takayuki Asao[5], Hiroyuki Kuwano[3], Takashi Nakano[1]

1 Department of Radiation Oncology, Gunma University Graduate School of Medicine, Maebashi, Japan, **2** Department of Human Pathology, Gunma University Graduate School of Medicine, Maebashi, Japan, **3** Department of General Surgical Science, Gunma University Graduate School of Medicine, Maebashi, Japan, **4** Department of Surgery, National University of Singapore, Singapore, Singapore, **5** Department of Oncology Clinical Development, Gunma University Graduate School of Medicine, Maebashi, Japan

Abstract

Objective: Enhancing immunologic responses, including human leukocyte antigen (HLA) class I expression on tumor cells and recognition and elimination of tumor cells by tumor-specific cytotoxic T lymphocyte (CTL), is considered a novel concept of radiotherapy. The present study examined patients who underwent preoperative hyperthermo-chemoradiotherapy (HCRT) for locally advanced rectal cancer to assess the correlation between HLA class I expression and clinical outcome.

Materials and Methods: Seventy-eight patients with locally advanced rectal adenocarcinoma who received preoperative HCRT were enrolled. The median age of the patients was 64 years (range, 33–85 years) and 4, 18, and 56 patients had clinical stage I, II and III disease, respectively. Formalin-fixed and paraffin-embedded tissues excised before and after HCRT were subjected to immunohistochemical analysis with an anti-HLA class I-A, B, C antibody. HLA class I expression was graded according to tumor cell positivity.

Results: In pre-HCRT, the number of specimens categorized as Grade 0 and 1 were 19 (24%) and 58 (74%), respectively. Only 1 patient (1%) showed Grade 2 expression. However, 6 (8%), 27 (35%), 7 (9%), and 12 (15%) post-HCRT specimens were graded as Grade 0, 1, 2, and 3, respectively. There was a significant increase in HLA class I expression in post-HCRT specimens ($p<0.01$). However, neither pre- nor post-HCRT HLA class I expression affected overall survival and distant metastasis-free survival in clinical stage III patients. Univariate analysis revealed that Post-HCRT HLA class I expression showed a significant negative relationship with LC ($p<0.05$). Nevertheless, multivariate analysis showed that there was no correlation between HLA class I expression and clinical outcome.

Conclusion: HCRT increased HLA class I expression in rectal cancer patients. However, multivariate analysis failed to show any correlation between the level of HLA class I expression and prognosis.

Citation: Sato H, Suzuki Y, Ide M, Katoh T, Noda S-e, et al. (2014) HLA Class I Expression and Its Alteration by Preoperative Hyperthermo-Chemoradiotherapy in Patients with Rectal Cancer. PLoS ONE 9(9): e108122. doi:10.1371/journal.pone.0108122

Editor: Torbjörn Ramqvist, Karolinska Institutet, Sweden

Received March 27, 2014; **Accepted** August 20, 2014; **Published** September 26, 2014

Data Availability: The authors confirm that all data underlying the findings are fully available without restriction. Data are available from the Gunma University Graduate School of Medicine Institutional Data Access/Ethics Committee for researchers who meet the criteria for access to confidential data.

Funding: The authors have no support or funding to report.

Competing Interests: The authors have declared that no competing interests exist.

* Email: syoshi@gunma-u.ac.jp

Introduction

Accumulating evidence supports the importance of cell-mediated immunity for controlling tumor growth and eliminating distant metastases [1]. Human leukocyte antigen (HLA) class I molecules and tumor antigen-specific cytotoxic T lymphocytes (CTL) play crucial roles in these responses. HLA class I molecules expressed by tumor cells present tumor-derived antigens to CTL, which then kill the target cells [2]. Many studies report a significant correlation between clinical prognosis and the expression of HLA class I by esophageal, non-small cell lung, head and neck squamous cell, and bladder cancers [3–8]. Moreover, the majority of these reports conclude that patients with low HLA class I-expressing cancers have a poorer prognosis than those with high-expressing cancers.

Radiotherapy is a major form of anti-cancer therapy, and is used to treat many types of cancer, regardless of clinical stage. It is generally accepted that irradiation induces cell death via apoptosis and/or necrosis by damaging (either directly or indirectly) DNA. However, recent studies suggest that radiation-induced immuno-

genic cell death is a concept different from the more "traditional" radiation-induced cell death [9–11]. The concept underlying radiation-induced immunogenic cell death is based on the induction of anti-tumor immune CTL responses by radiotherapy with modification of the immunogenic epitopes on tumor HLA class I molecules. Radiotherapy increases the expression of HLA class I molecules by human melanoma cells and by kidney and subcutaneous cells in HLA-A2 transgenic mouse [12]. By contrast, Speetjens et al. reported that irradiation did not effect HLA class I expression by rectal cancer cells [13]. However, few reports have examined the correlation between radiotherapy and HLA expression on tumor cells in a clinical setting [12,14,15]. Moreover, to the best of our knowledge, no studies have examined changes in HLA class I expression by tumor cells in the same patient before and after radiotherapy.

We previously treated rectal cancer patients with preoperative hyperthermo-chemoradiotherapy (HCRT) for several years and reported the clinical outcomes [16,17]. Here, we obtained samples from the same patients to examine (i) HLA class I expression on rectal cancer cells, (ii) changes in HLA class I expression induced by HCRT, and (iii) the relationship between HLA class I expression and prognosis.

Materials and Methods

Ethics statement

All patients provided their written informed consent to participate in this study. This study was approved by the institutional review board of Gunma University Graduate School of Medicine, Gunma, Japan (IRB approval number is 1051). Anonymity of the patients was preserved.

Patients and specimens

Seventy-eight patients with locally advanced rectal adenocarcinoma, who were consecutively treated with HCRT followed by surgery at Gunma University Hospital between 2003 and 2011, were enrolled in the study. Pre- and post-HCRT specimens were available for all patients.

The characteristics of the patient's and the tumors are summarized in Table 1. The median age of the patients at the start of HCRT was 64 years (range, 33–85 years). The mean and median follow up periods were 45 and 40 months (range, 3–103 months), respectively. For diagnostic workup, all patients underwent computed tomography (CT) of the abdomen and thorax to facilitate staging of regional and distant metastases. T stage was determined by CT and magnetic resonance imaging (MRI), particularly T2 weighted images, according to the TNM Classification of Malignant Tumors (UICC, 7th edition). Overall, 4, 18 and 56 patients were classified with stage I, II and III disease, respectively. Samples from the 56 patients with stage III disease were further examined to determine the correlation between HLA class I expression and prognosis.

Tissue specimens were excised endoscopically from rectal tumors before HCRT and then surgically after HCRT (median, 10 weeks; mean, 12 weeks; range, 1–54 weeks). Excised tissues were then fixed in 10% formalin for 24 h and embedded in paraffin. HLA class I expression was examined by immunohistochemistry.

Treatments

All 78 patients underwent preoperative HCRT, as previously reported [16]. Briefly, external beam radiotherapy (X rays; 10 MV) was delivered using an anteroposterior or three- or four-field box technique. The clinical target volume (CTV) comprised the primary tumor and the entire mesorectal tissue. The total radiation dose was 40–54 Gy (median, 50 Gy), with daily fractions

Table 1. Patient and tumor characteristics.

Patient characteristics	
Age (years)	
Median (range)	64 (33–85)
Gender	
Male	55 (71%)
Female	23 (29%)
Tumor stage	
T1	0 (0%)
T2	9 (12%)
T3	47 (60%)
T4a	12 (15%)
T4b	10 (13%)
Lymph-node metastasis	
N0	21 (27%)
N1	28 (36%)
N2	29 (37%)
Clinical stage	
1	4 (5%)
2	18 (23%)
3	56 (72%)

doi:10.1371/journal.pone.0108122.t001

Table 2. Relationship between pre-HCRT HLA class I expression and patient/tumor characteristics.

		Grade of HLA class I expression				
	Patient no. (%)	0	1	2	3	P-value
		No. (%)	No. (%)	No. (%)	No. (%)	
All	78	19 (24)	58 (74)	1 (1)	0 (0)	
Gender						
Male	55 (71)	15 (27)	40 (72)	0 (0)	0 (0)	0.68
Female	23 (29)	4 (17)	9 (78)	1 (4)	0 (0)	
Age						
<60	27 (35)	2 (7)	24 (89)	1 (4)	0 (0)	<0.05
≥60	51 (65)	17 (33)	34 (67)	0 (0)	0 (0)	
T stage						
1	0 (0)	0 (0)	0 (0)	0 (0)	0 (0)	0.17
2	9 (12)	0 (0)	9 (100)	0 (0)	0 (0)	
3	47 (60)	16 (34)	30 (64)	1 (2)	0 (0)	
4a	12 (15)	2 (17)	10 (83)	0 (0)	0 (0)	
4b	10 (13)	1 (10)	9 (90)	0 (0)	0 (0)	
N stage						
0	21 (27)	6 (29)	14 (67)	1 (5)	0 (0)	0.60
1	28 (36)	7 (25)	21 (75)	0 (0)	0 (0)	
2	29 (37)	6 (21)	23 (79)	0 (0)	0 (0)	
TNM stage						
I	4 (5)	0 (0)	4 (100)	0 (0)	0 (0)	0.21
II	18 (23)	6 (33)	11 (61)	1 (6)	0 (0)	
III	56 (72)	13 (23)	43 (77)	0 (0)	0 (0)	

HCRT, hyperthermo-chemoradiotherapy; HLA, human leukocyte antigen.
doi:10.1371/journal.pone.0108122.t002

of 2 Gy. Seventy-four patients also received 5-fluorouracil (5-FU) and Levofolinate, three received UFT and leucovorin, and one received Capecitabine.

Hyperthermia treatment was performed on a weekly basis (2–6 sessions (median, 5 sessions) each lasting 30 min) using capacitive heating equipment and a radiofrequency of 8 MHz (Thermotron-RF 8, Yamamoto Vinita Co. Ltd., Japan).

Surgery (mainly total mesorectal excision) was performed at 1–54 weeks (median, 10 weeks) after the completion of HCRT. Seventy-five patients (96%) underwent surgery within 17 weeks. Several patients who showed a clinical complete response to HCRT refused surgery; therefore, surgery was performed in only 3 patients (4%) of patients after more than 34 weeks.

Immunostaining for HLA class I

Formalin-fixed and paraffin-embedded specimens were used for immunohistochemical analysis. Tissue sections were deparaffinized and subjected to antigen retrieval with epitope retrieval solution (Target Retrieval Solution, Citrate pH 6; Dako, Glostrup, Denmark) at 121°C for 20 min. Endogenous peroxidase activity was blocked by Dako REAL (Dako). A primary antibody against the HLA class I-A, B, C heavy chain, EMR8-5 (Hokudo, Sapporo, Japan), which does not recognize the HLA class I heavy chain-β2-microglobulin-peptide complex, was diluted (1:70) in Antibody Diluent Solution with Background Reducing Components (Dako) and incubated with the tissue sections at 4°C overnight [18]. The sections were then incubated with a Histofine Simple Stain MAX-PO kit (Nichirei, Tokyo, Japan) for 30 min. Finally, the sections were treated with 3, 30-diaminobenzidine (DAB, Dako) for 1 min, and counterstained with hematoxylin. Specimens of normal lymph node served as positive controls. The isotype matched irrelevant immunoglobulin (Negative Control Mouse IgG1; Dako) was used as the negative control.

Two authors (HS and MI, both blinded to the clinical and pathological data) assessed HLA class I positivity in a semi-quantitative manner. Staining was classified as follows: Grade 0, < 10% stained cells; Grade 2, 10–50% stained cells; Grade 3, 50–90% stained cells; Grade 4, >90% stained cells. The relationship between HLA class I expression and clinical prognosis was assessed by dividing the post-HCRT specimens into two groups, as previously described [6,13,19]: Grades 0–1 and Grades 2–3. The relationship between HLA class I expression and clinical prognosis was not examined in pre-HCRT specimens because only one patient showed Grade 2–3 expression prior to HCRT.

Statistical analysis

Survival was measured in days, starting from Day 1 of HCRT to the time of death or final follow up. Univariate analysis of the actuarial overall survival rate (OS), the local control rate (LC), and the distant metastasis-free survival rate (DMFS) for each clinicopathological factor were analyzed using the Kaplan-Meier method, and differences between survival curves were analyzed using the log-rank test. Multivariate analyses using Cox's proportional hazards model were performed to examine the correlation between prognosis and multiple clinicopathological variables. Differences in HLA class I expression between pre- and

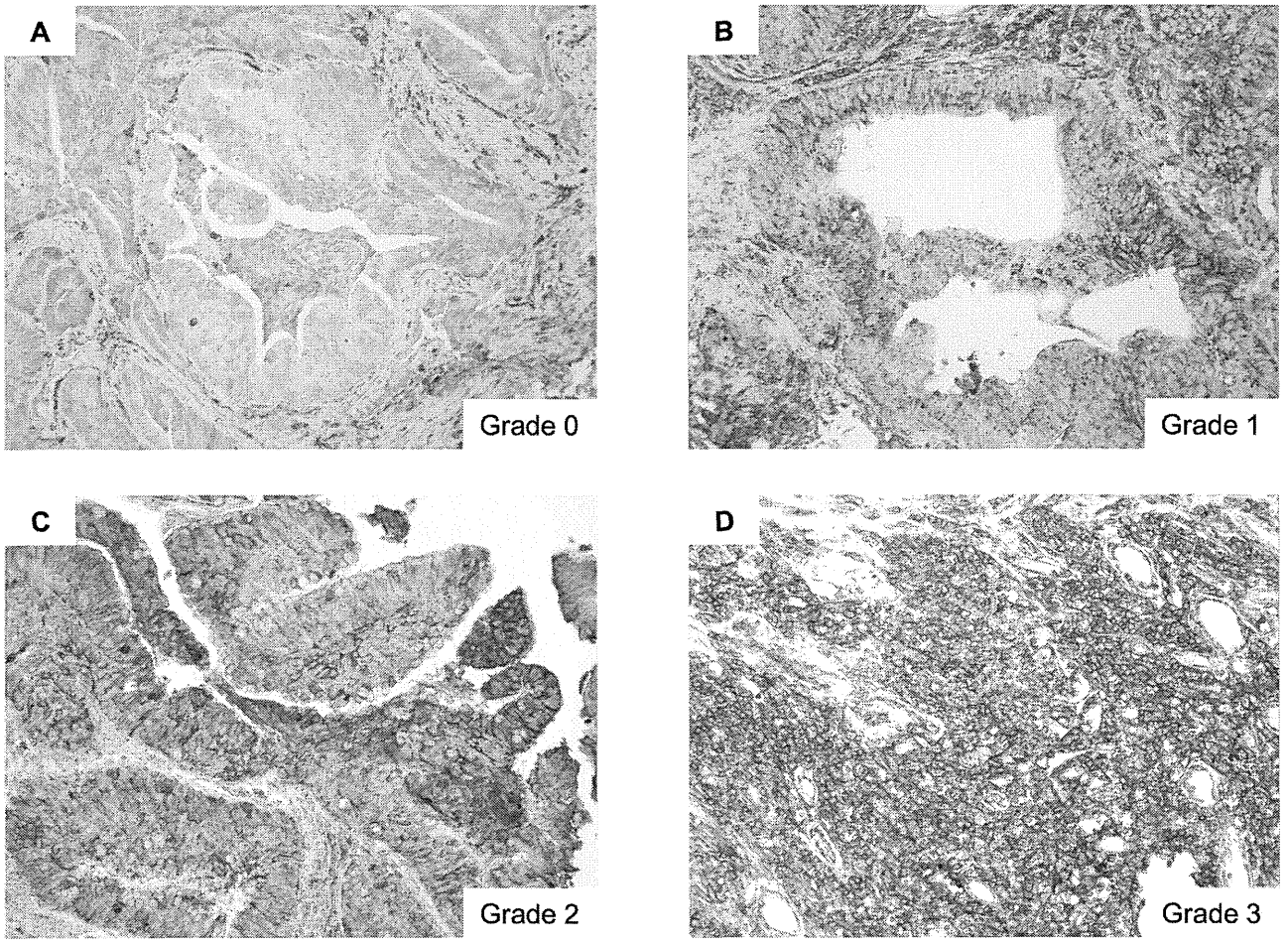

Figure 1. Human leukocyte antigen (HLA) class I expression in tumor cells. Representative images showing HLA class I expression by rectal cancer cells. A, Grade 0 expression. B, Grade 1 expression. C, Grade 2 expression. D, Grade 3 expression. Magnification, ×200.
doi:10.1371/journal.pone.0108122.g001

post-HCRT specimens were examined using the Wilcoxon signed rank test. Differences were considered significant at $P<0.05$. All statistical analyses were performed using SPSS software, version 21 (SPSS Japan Inc., Tokyo, Japan).

Results

HLA class I expression

Figure 1 shows HLA class I expression by rectal tumor cells. The number of pre-HCRT specimens categorized as Grade 0, 1, 2, and 3 was 19 (24%), 58 (74%), 1 (1%), and 0 (0%), respectively. The number of post-HCRT specimens categorized as Grade 0, 1, 2, and 3 was 6 (8%), 27 (35%), 7 (9%), and 12 (15%), respectively. Twenty-six patients (33%) showed a pathological complete response (pCR) post-HCRT. Table 2 shows that HLA class I expression correlated with patient age (<60 *vs.* ≤60), but not with other any other tumor characteristics or disease stage.

Changes in HLA class I expression induced by HCRT

Overall, 26 patients achieved pCR after HCRT. Changes in HLA class I expression were evaluated in tumor samples from the remaining 52 patients. Of these, 26 (50%) showed increased HLA class I expression, 3 (6%) showed reduced expression and 23 (44%) showed no change. The increase in HLA class I expression after HCRT was significant ($p<0.01$) (Figure 2). Of the 26 patients that achieved pCR, 5 (19%) showed Grade 0 expression pre-HCRT and 21 (81%) showed Grade 1 expression. There was no significant correlation between the Grade of HLA class I expression pre-HCRT and pCR.

Correlation between HLA class I expression and prognosis

The 5 year OS, LC, and DMFS for all 78 patients with Grade 0–1 post-HCRT HLA class I expression were 76%, 94%, and 76%, respectively, whereas the 5 year OS, LC, and DMFS of patients with Grade 2–3 post-HCRT HLA class I expression were 79%, 74%, and 79%, respectively (Table 3). There was no significant correlation between the three outcome parameters and the Grade of HLA class I expression. The pCR induced by HCRT showed a significant relationship with good LC ($p<0.05$).

Next, we further examined samples from the 56 patients with stage III disease to determine the correlation between HLA class I expression and prognosis. The 5-year OS, LC, and DMFS for stage III patients with Grade 0–1 post-HCRT HLA class I expression were 70%, 100%, and 70%, respectively, and the 5-year OS, LC, and DMFS for patients with Grade 2–3 post-HCRT HLA class I expression were 92%, 77%, and 85%, respectively (Figure 3). Post-HCRT HLA class I expression showed a

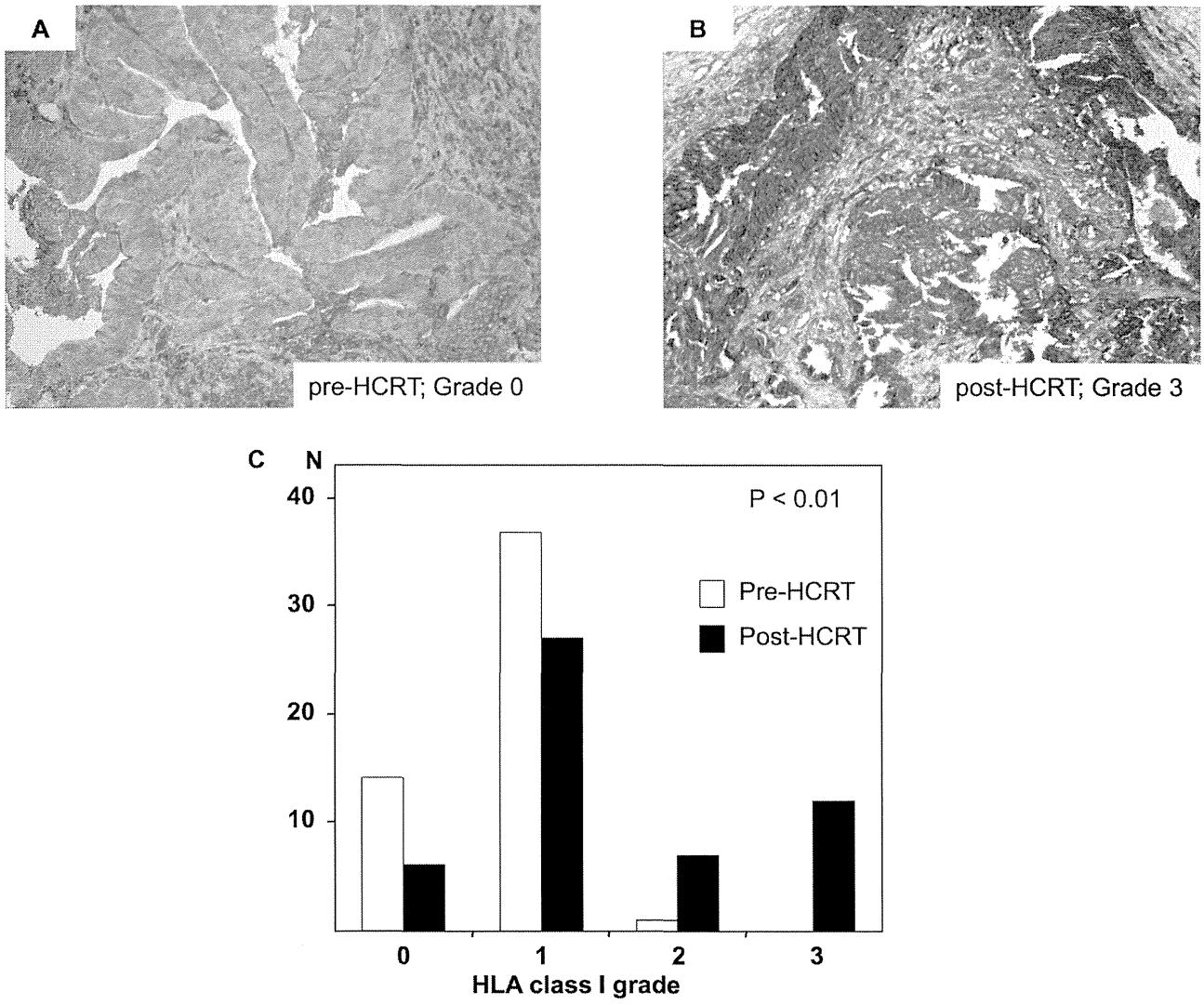

Figure 2. Changes in Human leukocyte antigen (HLA) class I expression after preoperative hyperthermo-chemoradiotherapy (HCRT). Grades of HLA class I expression in samples from the same patient. A, pre-HCRT specimen; Grade 0. B, post-HCRT specimen; Grade 3. Magnification, ×200. C, HLA class I expression in pre- and post-HCRT specimens. Predictive value was tested using the Wilcoxon signed rank test. doi:10.1371/journal.pone.0108122.g002

significant negative relationship with LC ($p<0.05$). However, multivariate analysis showed that none of the variables correlated with clinical prognosis (Table 4).

We next investigated examined whether the increase in HLA class I expression induced by HCRT improved the clinical outcome for stage III patients. The 5-year OS and DMFS for the "increased" group and the "constant or decreased" group were 77% and 78% ($p = 0.97$) and 71% and 78% ($p = 0.66$), respectively. There was no significant correlation between changes in HLA class I expression and OS and DMFS. On the other hand, the 5-year LC for the "increased" group and the "constant or decreased" group was 82% and 100%, respectively ($p = 0.04$). The LC of the "increased" HLA class I expression group was significantly worse than that of "constant or decreased" expression group.

Discussion

The main findings of the present study were as follows: (i) 19 (24%) and 58 (74%) of tumor tissue samples from patients with rectal adenocarcinoma showed Grade 0 (<10%) or Grade 1 (10–50%) expression of HLA class I, respectively; (ii) preoperative HCRT led to a significant increase in HLA class I expression; and (iii) multivariate analysis showed no significant positive association between HLA class I expression and survival.

Speetjens et al. examined the expression of HLA class I molecules in rectal cancer [13]. They categorized HLA class I expression as follows: absent (no expression), negative (0–50% positive cells), and positive (51–100% positive cells). They reported that 9.7%, 32%, and 58% of specimens were categorized as absent, negative, or positive, respectively when stained for the HLA class I antigen by using anti-HLA antibody, HCA2, but that 2.1%, 21%, and 77% were absent, negative, or positive, respectively, when stained for the HLA class I antigen by using anti-HLA antibody, HC10. Only one patient in the present study

Table 3. Univariate analysis of 5 year survival rates after hyperthermo-chemoradiotherapy (HRCT).

Factors	N (%)	OS		LC		DMFS	
		Rate (%)	P-value	Rate (%)	P-value	Rate (%)	P-value
Age							
<60	27 (35)	85	0.32	93	0.65	78	0.95
≥60	51 (65)	77		90		80	
Gender							
Male	55 (71)	78	0.66	87	0.08	82	0.49
Female	23 (30)	83		100		74	
Clinical stage							
1	4 (5)	100	0.55	75	0.19	100	0.63
2	18 (23)	72		83		78	
3	56 (80)	80		95		79	
HLA (Pre-HCRT)							
Grade 0, 1	77 (99)	79	0.56	91	0.73	81	0.06
Grade 2, 3	1 (1)	100		100		0	
HLA (Post-HCRT)							
Grade 0, 1	33 (64)	76	0.60	94	0.86	76	0.63
Grade 2, 3	19 (37)	79		74		79	
Pathological effect							
pCR	26 (33)	85	0.42	100	<0.05	85	0.55
No pCR	52 (67)	77		87		77	

OS, overall survival; LC, local control; DMFS, distant metastasis-free survival; HLA, human leukocyte antigen.

doi:10.1371/journal.pone.0108122.t003

Table 4. Multivariate analysis of 5 year survival rates after hyperthermo-chemoradiotherapy (HCRT).

Factors	OS		LC		DMFS	
	HR (95% CI)	P-value	HR (95% CI)	P-value	HR (95% CI)	P-value
Age (<60 or≥60)	0.82 (0.20–3.30)	0.79	1.18 (0.10–13.49)	0.89	0.93 (0.25–3.45)	0.92
Gender	0.86 (0.39–1.91)	0.72	0.00 (0.0–4.73E+135)	0.97	1.21 (0.61–2.41)	0.58
HLA class I (post-HCRT)	4.62 (0.57–37.47)	0.15	0.00 (0.0–7.68E+232)	0.96	2.26 (0.46–11.03)	0.31

OS, overall survival; LC, local control; DMFS, distant metastasis-free survival; CI, confidence interval; HLA, human leukocyte antigen; HR, Hazard ratio.
doi:10.1371/journal.pone.0108122.t004

showed >50% HLA class I positivity. This discrepancy may be partly explained by three factors. First, the primary monoclonal anti-HLA class I antibodies were different. They used HCA2 (which reacts with HLA-A (not HLA-A24), HLA-B73, and HLA-C molecules as well as HLA-E, HLA-F and HLA-G antigens), and HC10 (which reacts with HLA-B and HLA-C molecules and HLA-A10, -A28, -A29, -A30, -A31, -A32 and -A33 heavy chains) as the primary antibodies. However, we used EMR8-5, which reacts with HLA-A*2402, A*0101, A*1101, A*0201, A*0207, B*0702, B*0801, B*1501, B*3501, B*4001, B*4002, B*4006, B*4403, Cw*0102, Cw*0801, Cw*1202, and Cw*1502, as the primary antibody [18]. Second, semi-quantitative assessment is not the most accurate way to evaluate HLA class I expression. Finally, the differences may be explained by the "cancer immunoediting concept" proposed by Dunn, which describes the tumor alteration process consisted by three sequential phases (elimination, equilibrium and escape) to be acceptable to the immune system [20]. In this concept, the developing tumor cell had been eliminated by immune system before they become clinically apparent (elimination), however, a rare tumor cell was not killed by immune response, and consequently, these tumor cells emerge to cause clinically apparent disease (equilibrium and escape). Therefore, advanced cancer has tendency of low antigenic condition. Also, compared with Speetjens's study, the present study involved more patients with locally advanced rectal adenocarcinoma (72% of patients had stage III disease). Thus, we may have found lower levels of HLA class I expression. According to the "cancer immunoediting concept", HLA class I expression on tumor cells decreases with advancing stage.

Few reports have examined radiation-induced changes in HLA class I expression at different clinical phases; however, it has been demonstrated *in vitro* [12,14,15,21]. Speetjens et al., found also no significant differences in HLA class I expression in tumor samples from patients treated with or without irradiation [13]. By contrast, we found that HLA class I expression in rectal cancer cells increased after HCRT and this discrepancy might be due to the radiation dose, the interval between radiotherapy and surgery, or to the different analysis methods employed. Speetjens et al., treated one group of patients with 25 Gy per five fractions within 10 days of surgery and then compared HLA expression in tumor cells from irradiated and non-irradiated patients. By contrast, we treated patients with 50 Gy per 25 fractions within 5 weeks of surgery, and the median interval between radiotherapy and surgery was 10 weeks. We then compared HLA class I expressions on tumor cells from pre- and post-HCRT specimens from the same patients. Reits et al. reported that irradiation led to a dose-dependent increase in the levels of intracellular peptides derived from existing proteins and increased protein synthesis via mTOR activation. This resulted in an increase in MHC class I expression. However, the optimal dose/fraction and the interval between irradiation and evaluation for the highest level of HLA class I expression in the clinical phase is unknown.

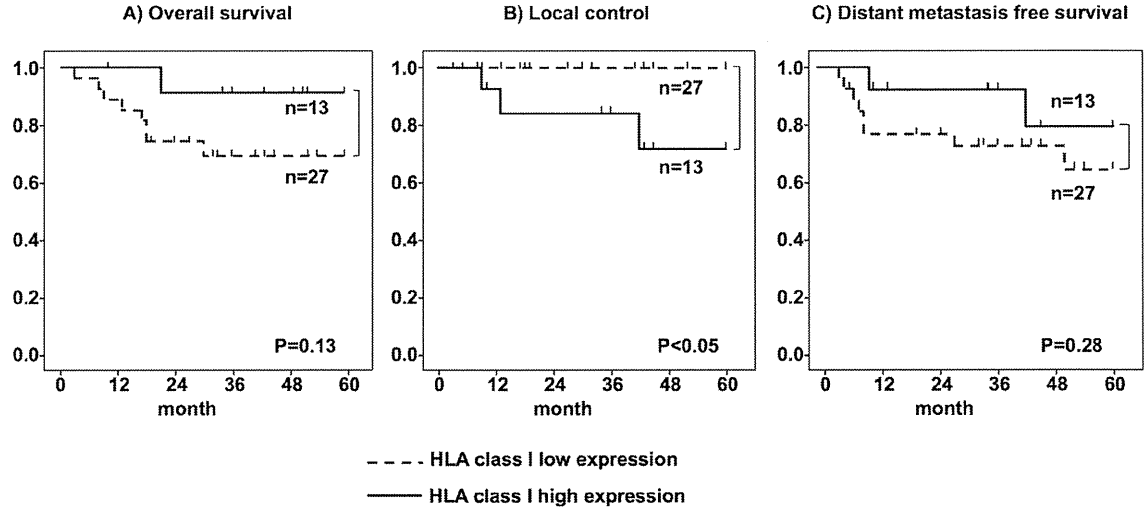

Figure 3. Relationship between Human leukocyte antigen (HLA) class I expression and clinical outcome. The clinical outcomes of 56 patients with stage III disease. (A; overall survival, B; local control, and C; distant metastasis-free survival). Low HLA class I expression: Grades 0 and 1; high expression: Grades 2 and 3.
doi:10.1371/journal.pone.0108122.g003